Digital Discovery

ROYAL SOCIETY OF CHEMISTRY

PAPER

View Article Online
View Journal | View Issue

Open Access Article. Published on 27 May 2025. Downloaded on 1/29/2026 3:29:41 AM.
This article is licensed under a Creative Commons Attribution 3.0 Unported Licence.

Check for updates

Cite this: *Digital Discovery*, 2025, **4**, 1602

Precursor reaction pathway leading to $BiFeO_3$ formation: insights from text-mining and chemical reaction network analyses†

Viktoriia Baibakova,[a] Kevin Cruse,[a] Michael G. Taylor,[b] Carolin M. Sutter-Fella,[a] Gerbrand Ceder,[a] Anubhav Jain[a] and Samuel M. Blau *[a]

Received 19th April 2025
Accepted 13th May 2025

DOI: 10.1039/d5dd00160a

rsc.li/digitaldiscovery

$BiFeO_3$ (BFO) is a next-generation non-toxic multiferroic material with applications in sensors, memory devices, and spintronics, where its crystallinity and crystal structure directly influence its functional properties. Designing sol–gel syntheses that result in phase-pure BFO remains a challenge due to the complex interactions between metal complexes in the precursor solution. Here, we combine text-mined data and chemical reaction network (CRN) analysis to obtain novel insight into BFO sol–gel precursor chemistry. We perform text-mining analysis of 340 synthesis recipes with the emphasis on phase-pure BFO and identify trends in the use of precursor materials, including that nitrates are the preferred metal salts, 2-methoxyethanol (2 ME) is the dominant solvent, and adding citric acid as a chelating agent frequently leads to phase-pure BFO. Our CRN analysis reveals that the thermodynamically favored reaction mechanism between bismuth nitrate and 2ME interaction involves partial solvation followed by dimerization, contradicting assumptions in previous literature. We suggest that further oligomerization, facilitated by nitrite ion bridging, is critical for achieving the pure BFO phase.

1 Introduction

Bismuth ferrite ($BiFeO_3$, or BFO) is a well-studied multiferroic material with significant applications in sensors, memory devices, and spintronics.[1,2] Perovskite BFO thin films have attracted considerable interest as multiferroic perovskites and a semiconductor alternative to lead-based perovskite solar cells. The crystallinity and crystal structure of BFO are key factors influencing its functional properties, which highlights the importance of the synthesis process.[2,3] Several methods, including sol–gel, hydrothermal, and solid-state techniques, have been employed to synthesize BFO.[4–9] Among these, sol–gel synthesis is particularly advantageous for growing single-phase films due to its ability to achieve uniform composition at the molecular level.[10] In this process, precursor materials are mixed in solution, followed by deposition, spin-coating, and temperature treatment.[1,7–9]

However, challenges remain in designing sol–gel protocols to achieve target outcomes.[10,11] Achieving a pure crystalline BFO phase is a topic of ongoing investigation, as even small changes in sol–gel protocol conditions can lead to different structures.[12,13] Variations in precursors, ratios, pH, temperature, time, pressure, atmosphere, and other factors can produce a wide range of compounds, often resulting in BFO with impurity phases or the formation of an amorphous phase.[7–9,11] While most parameters can be numerically analyzed and sequentially optimized to identify cutoff values,[3,11] selecting precursor materials for sol–gel BFO synthesis is not straightforward due to the complex underlying chemical interactions within the precursor solution.[12,14] For example, although the most common sol–gel BFO precursor solution, comprising nitrate salts and 2ME, has been experimentally studied,[1,14] the specific reaction pathways involved have yet to be explored from a computational perspective.

To add insight into the impact of precursors on BFO phase formation and the reactions occurring in the precursor solution, we propose the combined use of text-mining[15,16] and Chemical Reaction Network (CRN) methods.[17–19] Our approach is outlined in Fig. 1. Text-mining facilitates the extraction of synthesis protocols and phase outcomes from scientific literature, providing a broad perspective on experimental trends.[11] By systematically analyzing 340 sol–gel synthesis recipes targeting phase-pure BFO thin films, we identified key trends in the choice of metal precursors, solvents, and additives as critical factors influencing outcome phase. This text-mining analysis further informs the selection of systems for CRN modeling[20] to explore the underlying chemical reaction pathways at a molecular level. Our study investigates the detailed reaction pathways and intermediate structures involved in BFO synthesis, modeling the energetics and viability of various synthesis

[a]*Lawrence Berkeley National Laboratory, 1 Cyclotron Rd, Berkeley, CA, 94720, USA. E-mail: smblau@lbl.gov*

[b]*Theoretical Division, Los Alamos National Laboratory, Los Alamos, NM 87545, USA*

† Electronic supplementary information (ESI) available. See DOI: https://doi.org/10.1039/d5dd00160a

© 2025 The Author(s). Published by the Royal Society of Chemistry

Open Access Article. Published on 27 May 2025. Downloaded on 1/29/2026 3:29:41 AM.
This article is licensed under a Creative Commons Attribution 3.0 Unported Licence.

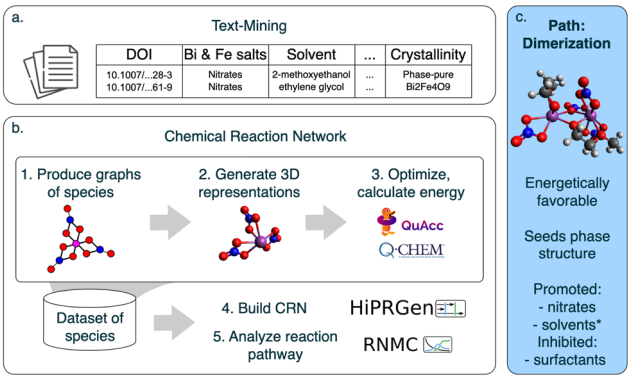

Fig. 1 Graphical abstract. To study the precursor solution, we used (a) text mining and (b) chemical reaction networks (CRNs). (c) Integrating text mining with CRNs provides insights into how precursor materials influence the reaction pathway. We hypothesize that nitrate salts and solvents that stabilize de-nitrated complexes promote dimerization. The dimerization suggests that surfactants obstruct the reaction, and our text-mining analysis supports this claim.

routes. Our findings highlight oligomerization and dimerization as dominant mechanisms, challenging the previously suggested hypothesis of a gradual nitrite-to-solvent replacement pathway. Based on these insights, we propose optimizing precursor materials by focusing on nitrate salts, selecting solvents stabilizing de-nitrated complexes, and avoiding surfactants.

This paper consists of the following parts. The Methods section describes in-detail the text-mining techniques and CRN analysis used to extract and model the synthesis data, as well as assumptions made regarding structural representation. In the Results section, we present the findings from the text-mining analysis and CRN simulations, including trends in precursor selection and reaction pathways. We emphasize the oligomerization pathway in the sol–gel process. In the Discussion section, we interpret our findings in the context of existing studies, explaining that nitrate salts and solvents that stabilize de-nitrated complexes can enhance oligomerization while surfactants tend to inhibit it, and explore the potential future implications of these results.

2 Methods

We used data-driven methods, text-mining and CRN, to study the molecular reactions at play in the precursor solution for BFO thin films. The general workflow is outlined in Fig. 1.

2.1 Text-mining

We used text mining to study the diversity of the precursor solution composition and establish the link between precursor materials and the resulting phase (Fig. 1a). We selected 178 scientific publications reporting sol–gel synthesis of BFO and targeted phase-pure perovskite thin films through a multi-step process. A keyword search of an in-house database containing nearly 5 million materials science articles published between 2000 and 2020 identified 82 196 papers discussing impurity phase formation. Chemical Named Entity Recognition was then used to extract relevant materials, narrowing the focus to BFO. Further filtering based on synthesis method and relevance to sol–gel-derived BFO thin films resulted in 121 suitable articles. To supplement our dataset with articles published after 2020, we scraped Web of Science, filtering for papers on sol–gel synthesis targeting BFO. This search yielded 57 additional papers. Publication selection is described in detail in our accompanying paper.[11]

Next, we manually extracted synthesis parameters and outcomes for 340 synthesis descriptions. Due to the complexity and variability of the synthesis descriptions and the limited automated capabilities at the time, we chose human-driven literature extraction which enabled us to capture nuanced insight that programmatic text-mining could not yet achieve. We extracted and tabulated all synthesis parameters mentioned in the experimental sections of selected papers, such as temperature, pH, time, concentration, *etc.*, and performed a comprehensive programmatic analysis in our accompanying paper.[11] However, in this work, we focus on precursor materials and output phases. To structure the data, we classified all materials (according to the claims of the authors and in a consistent way) into the following roles: metal source, solvent, chelating agent, dehydrating agent, or surfactant. We then conducted a statistical analysis to identify the most frequently used materials in each category, labeling less frequent materials as "other". See ESI† for the full list of materials and details of the analysis.

2.2 Assumptions about metal complexes

To describe the chemical reaction pathway for the BFO system using a data-driven CRN approach, we made several assumptions about metal complexes. We focus solely on Bi due to its similar chemical behavior with Fe[14] and to avoid computational complexity associated with Fe's incomplete d-shell. The Bi-metal ion core forms ionic and coordination bonds with inorganic (nitrite ion, nitric acid) and organic ($2ME_{dehydr}$ ion, 2ME) ligands. We assume a neutral precursor solution with Bi^{3+} charge, resulting in complexes with three ionic ligands and varying numbers of nonionic ligands. Ligands can be mono- or bi-dentate, influencing coordination geometry. Based on data from the Crystal Structure Database[21,22] (see ESI†), Bi^{3+} ions coordinated with oxygen exhibit ligand-dependent coordination with coordination number (CN) ranging from 4 to 9 and the median CN of 6. Thus, we do not limit the CN but set an initial coordination of 6 for bismuth nitrate. Water ligands were excluded as they tend to form hydrogen bonds with organic ligands rather than coordinate with Bi-metal centers, see ESI.†

2.3 Chemical reaction network

A Chemical Reaction Network (CRN) is a mathematical framework used to model and analyze chemical reactions, particularly in complex systems where experimental observations are difficult. CRNs allow for systematic exploration of chemical interaction spaces, enabling the identification of feasible reaction pathways and providing predictions of reaction outcomes.[17,20,23]

Open Access Article. Published on 27 May 2025. Downloaded on 1/29/2026 3:29:41 AM.
This article is licensed under a Creative Commons Attribution 3.0 Unported Licence.

A CRN consists of two main elements: a dataset of chemical species (including reactants, reaction intermediates, and products) and the reactions between them, characterized by parameters such as free energy changes and activation barriers. Thus, the reaction pathway is broken down into elementary reaction steps occurring between intermediate species with minimal changes in structure and composition in each elementary step. This allows CRNs to model the entire reaction landscape in detail and identify energetically favorable pathways.[24] The method is highly parallelizable and compatible with modern computational architectures, offering resource-efficient solutions for large-scale chemical systems and high-throughput studies.[19,25]

To study the chemical reaction space of bismuth nitrate dissolved in 2ME, we built a CRN (Fig. 1b) and used a BEP-type approximation to relate the Gibbs free energy to the activation energy as the reaction driving force. We started by preparing a dataset of species for CRN including partial ligand exchanges: we represented reactant molecules as molecular graphs using SCINE Molassmebler[26] and iteratively generated intermediate species toward the product (step 1). For each graph, we generated 3D conformers and pre-optimized them using Architector[27] and TBLite[28] (step 2). We selected three lowest energy conformers, optimized them and calculated thermodynamic potentials using QChem[29] and QuAcc[30] (step 3). We compiled this information into a comprehensive dataset of species and generated a dataset of reactions between them with High Performance Reaction Generation (HiPRGen)[31] (step 4). Lastly, we produced reaction pathway trajectories with Reaction Network Monte Carlo (RNMC)[31] (step 5). See more details on each step below. To handle structures with multiple Bi centers and bridging ligands, we performed steps 1 and 3 of the pipeline.

A chemical reaction network is defined by a set of species and reactions, and each run of RNMC produces a trajectory by selecting a reaction at every step; although no exhaustive method can address the vast space of possible complexes and reaction paths, the CRN approach captures as many possibilities as feasible, surpasses previous methods, and provides new insights.[24]

2.3.1 Step 1-dataset of species, producing intermediates. To populate the species dataset for CRN, we focused on Bi–O bond patterns and first generated the reaction intermediates as molecular graphs:[32] metal complexes with partial replacement of nitrite ligands in $[Bi(NO_3)_3]$ with 2ME solvent ligands. The latent molecular graph representation used only atomic bond information, treating a metal complex as a list of bonded atomic pairs without distinguishing between ionic and coordination bonds. This simplified the representation of metal complexes, making the algorithm more adaptable for different molecular systems. Using the SCINE Molassembler[26] package, we developed a fragmentation-recombination loop algorithm that allowed us to generate reaction intermediate molecular graphs, starting with the input molecular graph of $[Bi(NO_3)_3]$, see ESI† for details. In the fragmentation stage, we iterate through all Bi–O bonds in the input metal complex and break a single bond, generating a molecular graph of a complex fragment. In the recombination stage, we form a new Bi–O bond in each fragment graph either with existing ligands or by attaching another ligand (2 ME, $2ME_{dehydr}$ ion, nitrite ion, nitric acid). We removed isomorphs, charged species, and graphs with tridental ligands. To reduce computational load, we then discarded intermediates: (1) with ionic $2ME_{dehydr}$ attached only *via* methoxy oxygen ($-OCH_3$), assuming the alkoxide oxygen ($-O^-$) to be the preferred connection site; (2) with four or more nitrite ligands (nitrite ion and nitric acid) or four or more solvent ligands ($2ME_{dehydr}$ ion and 2ME). Since the used latent molecular graph representation ignores bond lengths and angles, we follow this step with 3D conformer generation.

2.3.2 Step 2-dataset of species, generation of 3D conformers. To complete the generation of intermediate species for the CRN dataset, we built 3D conformers from the latent molecular graph representations created in the previous step. The process of generating 3D configurations from molecular graphs is inherently complex due to the existence of multiple possible 3D conformers for a single graph. For this, we utilized the Python Architector package,[27] which specializes in generating 3D conformers for organometallic compounds by applying topological rules and incorporating experimental data on metal complexes. While SCINE Molassembler[26] also offers 3D molecule generation capabilities, Architector provides enhanced functionality, including various relaxation methods specifically designed for metal complexes, leading to more accurate and reliable molecular structures. This approach also helps mitigate the influence of input parameters on the selection of 3D conformers.

We converted Molassembler graphs into Architector's input format: dictionaries listing the metal core, coordination number (CN), and ligands in SMILES notation with bonding site indexes (ligands listed in ESI†). We ran Architector with force-field pre-optimization, the solvent set to "octanol" (approximating 2ME by dielectric constant), and requested 20 total metal-center symmetries. We used the Sella optimizer (from the Architector developer branch), which, although requiring 2–10 CPU node-hours per graph, yielded configurations more consistent with the input molecular graph and lower in energy compared to the default LBFGS optimizer.[33] We also set Architector to perform geometry relaxation with GFN2-xTB[34] and selected the 3 lowest-energy conformers based on xTB energy values for further DFT calculations. While satisfactory for this task, this method lacks support for oligomeric complexes; dimer structures were handled using SCINE Molassembler.

2.3.3 Step 3-dataset of species, free energy calculations. To obtain Gibbs free energies for species in the dataset, we followed the optimization-frequency-single point (opt-freq-sp) calculation workflow, automating it with QuAcc.[30] Metal complexes were generated with Architector (previous step), and ligand molecules were assembled using Avogadro.[35] We run geometry optimizations using DFT at the ωB97M-V/def2-SVPD[36,37] level with the PCM solvation model[38] in Q-Chem 6.0,[29] employing a dielectric constant of 16.93 for 2ME and the default PCM QChem parameters for all other settings. Although Q-Chem optimizations required 10–20 CPU node-hours per structure, inexpensive semi-empirical methods like xTB and

 © 2025 The Author(s). Published by the Royal Society of Chemistry

Open Access Article. Published on 27 May 2025. Downloaded on 1/29/2026 3:29:41 AM.
This article is licensed under a Creative Commons Attribution 3.0 Unported Licence.

TBLite[28] were insufficient for our structures. We performed vibrational analysis with TBLite at the GFN2-xTB level and discarded species with imaginary frequencies. Comparison of TBLite's enthalpy and entropy values with Q-Chem showed a variance within 5% (see ESI†), while reducing resource usage tenfold. We then refined energy values with single-point energy calculations at the ωB97M-V/def2-TZVPD level with PCM in Q-Chem and used these to calculate Gibbs free energy values.

Overall, we collected a species dataset with the following data: relaxed 3D molecule, energy, entropy, and enthalpy. We note that during the geometry relaxations some bonds were not preserved, and the molecule graphs were updated accordingly.

The species dataset for the CRN is illustrated in Fig. 2. The fragmentation-recombination loop generated 809 unique molecular graphs, which we reduced to 110 graph dictionaries with ligand-based filtering as described earlier. Adding graph dictionaries with higher Bi CN enhanced the dataset for the potential product study (P). Architector produced a total of 1900 pre-optimized structures. Running DFT optimization of the three lowest energy conformers resulted in 231 molecules with unique molecular graphs. The optimized structures exhibit CN ranging from 4 to 10 with a median of 6. The ratio of nitric to 2ME ionic ligands indicates a trend toward more structures with 2ME ligands, consistent with the expected reaction direction. The study of potential products resulted in seven 3D conformers with CN of 7 and 8, and free energy analysis demonstrated that adding a fourth neutral 2ME ligand to Bi coordinated with three 2ME ions is not thermodynamically beneficial (see ESI†), corroborating earlier claims on similar structures.[39]

2.3.4 Step 4-building CRN. Finally, to establish a set of chemical reactions and the relationships between reactants and products in the Bi nitrate and 2ME solution chemical reaction space, we built a CRN by systematically generating and filtering possible reactions between species in our dataset. We utilized the HiPRGen tool[31] with MPI4Py multi-node parallelization. We loaded a dataset with species information (relaxed 3D molecular structure, electronic energy, entropy, and enthalpy) into HiPRGen and updated molecular graphs for relaxed geometries using a Bi–O bond length cut-off of 3.4 Angstrom. Utilizing HiPRGen's flexibility, we configured species and reaction filters feasible for our task. Species filter rules included all dataset species and fragments resulting from the breaking of one or two bonds. Elementary reaction filter rules allowed reactions with $\Delta G < 5$ eV, discarded reactions with coexisting species (*e.g.*, A + B → A + C as A can be removed to form the simpler B → C reaction), rejected reactions separable by composition (*e.g.*, when an A + A → B + C can be broken into A → B and A → C), and permitted up to 4 total distinct bonds to be broken and formed in a single step. With HiPRGen, we enumerated all possible reactions between species and applied filters, disregarding reactions that do not meet our criteria, see ESI† for the list of the reactions. HiPRGen produced a total of 388 distinct reaction steps. We provide the full list of steps and their rates of occurrence in the ESI.†

2.3.5 Step 5-analyzing reaction pathways. To construct the full reaction pathways and consumption rates from CRN, we use the RNMC software.[31] We set the reaction barriers equal to the change in free energy at room temperature, assigning zero barriers to all energetically favorable reactions. We simulate the initial conditions for the Monte Carlo simulation with a ratio of bismuth nitrate to 2ME solvent molecules of 1 : 100. We run 100 trajectories of 10 000 steps each using GMC, Gillespie's next reaction simulator.[40]

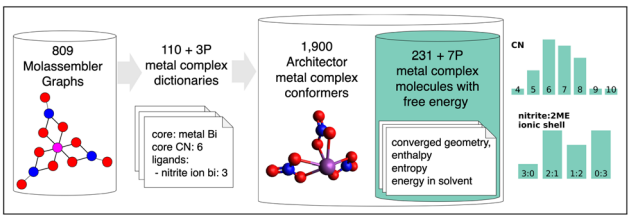

Fig. 2 Data flow in the generated CRN dataset follows the approach outlined in steps 1–3 described in the methods section. The dataset used in HiPRGen comprises 231 metal complexes with coordination numbers (CN) ranging from 4 to 10 and various ratios of nitrite to 2ME among the ionic ligands. 'P' denotes product structures.

2.4 Dimer study

To find the dimer lowest energy configuration, we followed steps 1–3 from the CRN box in Fig. 1 with several adjustments. We started with the molecule graph for the dimer-ready structure: $[Bi^{3+}(NO_3^-)_2(2ME^-)]$ determined in CRN analysis and connected two such graphs in order to form the dimer molecule graph using SCINE Molassembler. We built two different dimer molecular graphs, bridging with one and two nitrite ions and zero total charge, see ESI† for molecular graphs. Then, since Architector does not support multi metal complexes, we used SCINE Molassembler to generate 50 3D conformers and randomly chose 10 for each dimer graph. We followed with opt-freq-sp calculations in Q-Chem at the same level of theory as in original CRN step 3, and 17 dimer conformers converged. We chose the conformer with the lowest Gibbs free energy at room temperature, see ESI† for the full list of conformer energies and the lowest energy conformer XYZ.

3 Results

3.1 Text-mining

To study the diversity of precursor materials and establish a connection with the resulting BFO material phases in reported experiments, we text-mined 340 synthesis recipes targeting phase-pure BFO and analyzed the collected dataset (see the results of the text-mining analysis in Fig. 3). We categorized the resulting phases into three groups: pure crystalline phase (73%), impure crystalline phase (24%), and amorphous phase (3%). Metal precursor nitrates are used in 94% of the recipes, while the remaining 6% use other salts, which yield all three phase outcomes. Thus, we could not observe a statistically significant correlation between salt choice and phase outcome from our data. Next, we incorporated solvents into the resulting material phase analysis. Specifically, 2ME is used in 73% of

Open Access Article. Published on 27 May 2025. Downloaded on 1/29/2026 3:29:41 AM.
This article is licensed under a Creative Commons Attribution 3.0 Unported Licence.

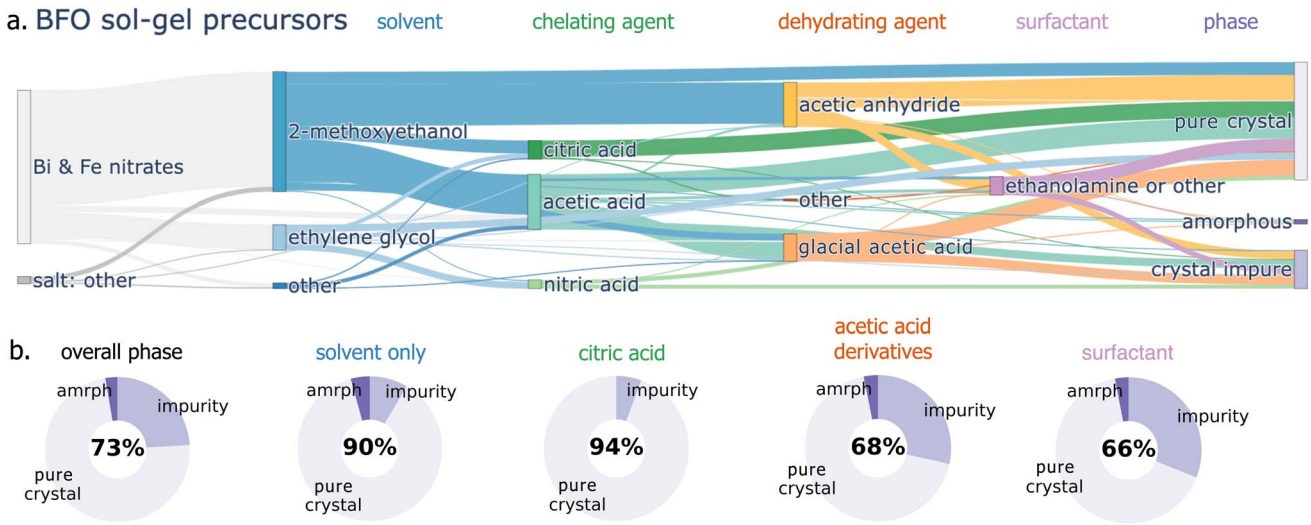

Fig. 3 (a) Precursor composition diagram from text-mined dataset. Vertical bars represent quantitative distribution of materials used in recipes. (b) Phase outcomes for different precursor materials. Solvent with no other additives leads to phase-pure crystalline BFO in 90% of cases. Addition of citric acid leads to a pure crystalline phase in 94% of cases. Acetic acid derivatives yield phase-pure BFO in 68% of cases. Overall portion of recipes reporting pure crystalline phase is 73%.

recipes, and ethylene glycol is used in 16% of the recipes. There are 50 recipes in our dataset that use only metal salts and solvents without other additives, and in 90% of those cases, they result in pure crystalline phase formation. These findings suggest that 2ME is the preferred solvent and is optimal for achieving a pure-phase crystalline BFO when no additional materials are included.

Chelating agent citric acid, used in 12% of the recipes, maintains high phase-pure crystalline BFO yield: among 40 recipes with salts, solvent, and citric acid (no additional materials), 94% result in phase-pure BFO. In contrast, other chelators such as more common acetic acid or nitric acid (used in 34% and 5% of recipes respectively), show less consistent results. Among 190 recipes that use acetic acid, glacial acetic acid or acetic anhydride (which forms acetic acid after interacting with water), only 68% lead to phase-pure BFO, while 29% yield impure crystalline phase. Among 18 recipes using nitric acid, only 55% yield pure phase, and 45% result in impurities formation. These findings suggest that citric acid is a more reliable chelating agent for pure BFO synthesis compared to acetic or nitric acid. Contrary to the expectations that surfactants enhance phase-pure BFO formation,[9,41] our analysis shows that their inclusion decreases the likelihood of achieving pure crystalline BFO phase: the fraction of recipes using surfactants and reporting phase-pure, impure, and amorphous phases is 66%, 31%, and 3% (with the overall recipes outcome phases fractions being 73%, 24%, and 3%), indicating that their role in phase purity enhancement is not straightforward.

To summarize out text-mining analysis, for researchers aiming to synthesize phase-pure BFO, we recommend using nitrate precursors, 2ME as the solvent, and citric acid as the chelating agent, while avoiding unnecessary additives that may introduce complexity without clear benefits.[10] Motivated by text-mining results, we selected the most common precursor, bismuth nitrate dissolved in 2ME, and performed a computational analysis of its reaction pathways. We apply CRN approach to investigate the reaction path in detail in the context of observations from text-mining.

3.2 Chemical reaction network

The CRN analysis of bismuth nitrate dissolved in 2ME, as illustrated in Fig. 4, distills the complex CRN down to a handful of critical reactions, capturing both expected and unexpected pathways. Previous literature[1,14] suggests that the complete replacement of nitrite ligands with 2ME ligands, as shown in Reaction (1), occurs before the formation of any oligomeric species on the way towards crystallization:

$$[Bi^{3+}(NO_3^-)_3] + 3\cdot 2ME \rightarrow [Bi^{3+}(2ME^-_{dehydr})_3] + 3HNO_3 \quad (1)$$

Surprisingly, our calculations show that this overall reaction is endergonic, with a change in Gibbs free energy of $\Delta G(1) = +0.89$ eV. However, the beginning of the path is energetically favorable. We call the exergonic part of the pathway "partial solvation", in which one nitrite ligand is replaced by one solvent ligand (see ESI†), as shown in Reaction (2):

$$[Bi^{3+}(NO_3^-)_3] + 1\cdot 2ME \rightarrow [Bi^{3+}(NO_3^-)_2(2ME^-_{dehydr})] + HNO_3 \quad (2)$$

In the CRN, Reaction (2) is composed of three elementary steps: solvation (3), H swap (4), acid detachment (5) as described with Reactions (3)–(5):

Solvation:

$$[Bi(NO_3^-)_3] + (2ME) \rightarrow [Bi(NO_3^-)_3(2ME)] \quad (3)$$

 © 2025 The Author(s). Published by the Royal Society of Chemistry

Open Access Article. Published on 27 May 2025. Downloaded on 1/29/2026 3:29:41 AM.
This article is licensed under a Creative Commons Attribution 3.0 Unported Licence.

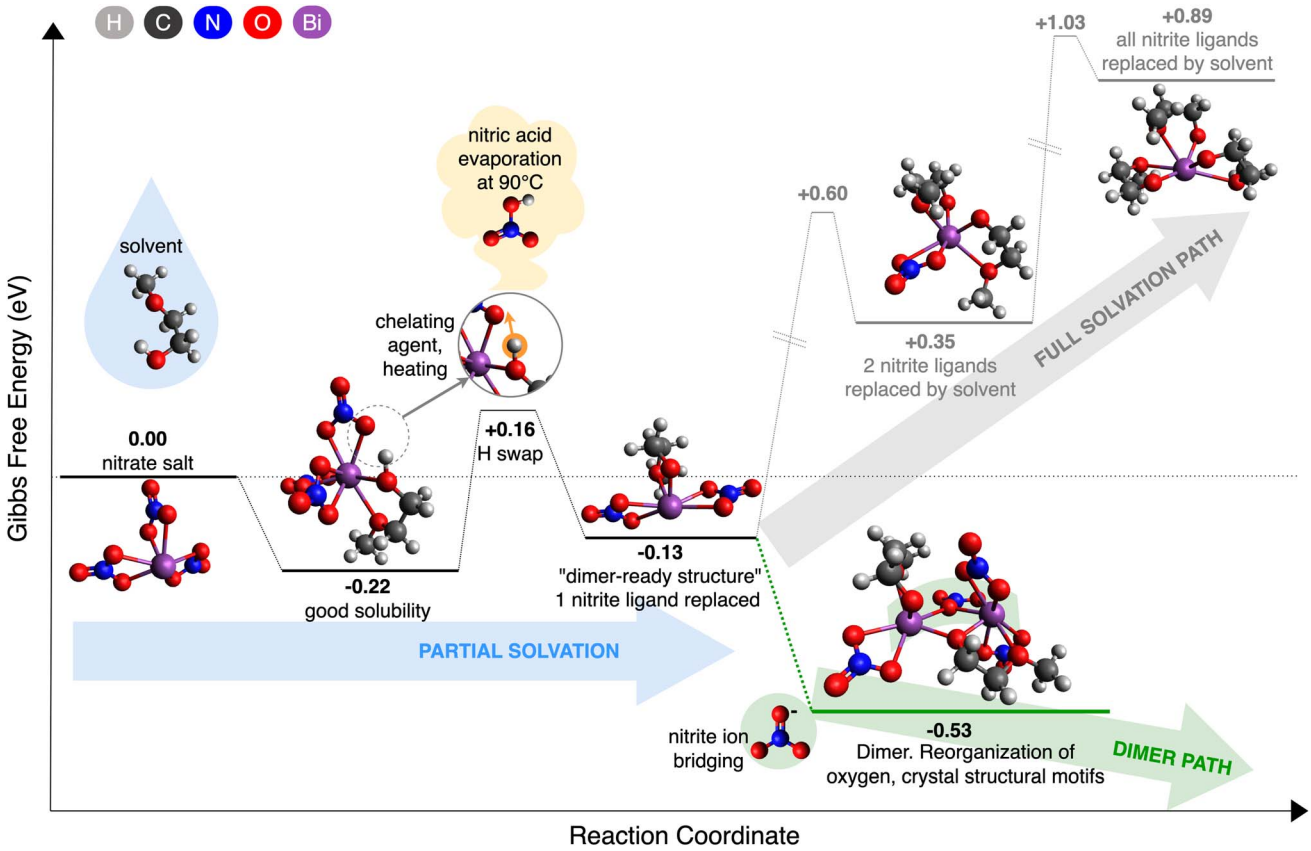

Fig. 4 Reaction path energy profile based on CRN analysis. The full solvation path is expected based on previous hypotheses but is found to be highly thermodynamically unfavorable. In contrast, the novel dimer path revealed by our analysis is thermodynamically favorable, suggesting a more likely route towards crystallization.

H swap:

$$[Bi(NO_3^-)_3(2ME)] \rightarrow [Bi(NO_3^-)_2(2ME^-_{dehydr})(HNO_3)] \quad (4)$$

Acid detachment:

$$[Bi(NO_3^-)_2(2ME^-_{dehydr})(HNO3)] \rightarrow [Bi(NO_3^-)_2(2ME^-_{dehydr})] + HNO_3 \quad (5)$$

The process begins with the solvation of the initial bismuth nitrate metal complex, where a neutral 2ME solvent molecule attaches to the complex. The attachment of 2ME is energetically favorable, with a solvation free energy of $\Delta G(3) = -0.22$, indicating good solubility, as expected. CRN analysis reveals that the optimized complex, $[Bi(NO_3^-)_3(2ME)]$, has a CN of 8, with 2ME forming two Bi–O bonds. This bi-dentate interaction significantly contributes to the stability of the complex. Following the initial solvation, a proton transfer, *i.e.* H swap, occurs from the hydroxyl group (–OH) of 2ME to a nitrite ligand. This step has an associated free energy change of $\Delta G(4) = +0.38$ eV. Despite being energetically unfavorable (endergonic), the overall free energy change relative to the initial state is $\Delta G = +0.16$, which is five times smaller than $\Delta G(1)$. Further, we know that heat is required to drive this process forward, so the presence of an intermediate endergonic step is unsurprising. Subsequently, the byproduct nitric acid detaches from the bismuth core with $\Delta G(5) < 0$, leading to the formation of a new complex, $[Bi(NO_3^-)_2(2ME^-_{dehydr})]$, referred to as the "dimer-ready structure" for reasons that will be clarified below. This structure is characterized by the replacement of one nitrite ligand with one solvent ligand, making it the final stable complex on the expected solvation pathway that is energetically lower than the initial state, see ESI† for the reaction report. After the formation of the "dimer-ready structure," the full solvation pathway continues with the substitution of the remaining two nitrite ligands with solvent molecules. However, these subsequent steps are increasingly endergonic, with significant energy costs, making the overall pathway thermodynamically unfavorable and thus highly unlikely to occur.

However, as illustrated in Fig. 4, our CRN analysis reveals that dimerization after partial solvation is exergonic, presenting a novel alternative mechanistic route towards crystallization that is vastly more thermodynamically favorable than the expected full solvation path. This "dimer path" can be described as two "dimer-ready structures" joining together as denoted by Reaction (6):

$$2[Bi(NO_3^-)_2(2ME^-_{dehydr})] \rightarrow [Bi_2(NO_3^-)_4(2ME^-_{dehydr})_2] \quad (6)$$

Open Access Article. Published on 27 May 2025. Downloaded on 1/29/2026 3:29:41 AM.
This article is licensed under a Creative Commons Attribution 3.0 Unported Licence.

where dimer formation is energetically favorable, with $\Delta G(6) = -0.4$. The dimer configuration we report features two Bi ions asymmetrically bridged by a nitrite ligand and a solvent ion ligand in a rhombic bonding motif. Additional Bi coordination sites are partially occupied by nitrites and solvent ions. We note that asymmetric bridging and rhombic bonding motifs were also reported in experimental investigations on similar dimeric complexes,[42,43] supporting the viability of our discovered pathway. Among the 17 tested dimer structures and all the structures in the CRN dataset, the dimer structure exhibited the lowest energy. In the context of reaction pathways, the dimer structure was also the most stable product (see ESI†).

4 Discussion

Through text mining with the emphasis on phase-pure BFO, we examined what precursor materials experimentalists select based on expected behaviors in the solution, specifically the selection of metal salt, solvent, chelating agent, dehydrating agent, and surfactant. Solvents, typically volatile long organic molecules, are expected to help with forming a dense, stable polymeric precursor.[1,14] Chelating agents, or chelators, are organic acids which should possess specific ligands that have high affinity and can bind/carry metal ions and are claimed to increase gel viscosity and encourage the formation of oligomeric structures.[1,44] Dehydrating agents are employed to remove excess water by bounding it, thus promoting homogeneity of the final gel.[1] The studies that employ surfactants commonly motivate it by the assumption that they improve phase purity by increasing gel homogeneity and promoting chemical reactions in it.[1]

In our chosen precursor of study, Bi nitrate with 2ME as motivated by text mining, the reaction path was previously claimed to proceed as gradual replacement of nitrites with solvent ligands within a single-metal complex.[1,14] There have been several experimental efforts where the BFO precursor was studied with Fourier Transform Infrared Spectroscopy (FTIR) for the bond presence before and after the reaction.[14] The analysis indicated Bi–nitrite bonds before the reaction and Bi–2ME bonds after. The possible reaction pathway was described as the complete substitution of nitrite ligands with solvent for each Bi complex *via* gradual ligand replacement.[1,14] This route is what we call "full solvation" and is described by Reaction (1).

We contradict an existing hypothesis that the chemical reaction in BFO precursor occurs as a gradual replacement of nitrite ligands with 2ME ligands within one complex. We find this reaction to be overall endergonic with $\Delta G(1) = +0.89$ eV, making it energetically unfavorable. The estimated temperature for this reaction to proceed, from the formula $T = \Delta H_{rxn}/\Delta S_{rxn}$, is 300 °C, see ESI.†. However, while it was previously experimentally demonstrated that the precursor requires heating for bonds to change, the reported temperature was much lower – about 90 °C.[14] Further, our CRN analysis reveals that every step of the "full solvation" route after the initial 2ME-nitrite swap is energetically unfavorable.

We instead hypothesize that the chemical reaction in the BFO precursor occurs through dimerization with both nitrite and solvent ligands coordinating Bi metal cores. Our CRN analysis revealed the first step of the oligomerization chain: formation of a dimer. The dimer configuration we report exhibits asymmetrical bridges involving both nitrite ions and solvent ions, consistent with a previous study which found that Bi complexes form dimeric structures with asymmetrically bridging ligands and additional coordination sites partially occupied by solvent molecules.[43] This aspect of solvent involvement aligns with the subproducts we identified by the CRN. Hence, selecting the right precursor materials and their treatment is crucial for successful oligomerization. Returning to our findings, since we established dimerization as the preferential pathway in the precursor, we hypothesize that additives may lead to deviations from this route and result in impurity phase formation in BFO synthesis.

It was previously suggested that oligomer formation determines the structural motifs of the resultant BFO phase,[14] and our results are consistent with this statement. In the BFO crystal, Bi–O–Bi bonds exhibit a rhombohedral arrangement with oxygen ions fourfold coordinated with metals. This motif can already be observed in the dimer structure as illustrated in Fig. 5. Two "dimer-ready structures" are linked with Bi–nitrite–Bi and Bi–$2ME_{dehydr}$–Bi bonds with oxygens following a similar rhombohedral pattern. We expect that as more Bi complexes participate, oligomerization proceeds, forming spatial arrangement of bridges to bring oxygen ions to a fourfold coordination state and BFO phase seeding.

To strengthen the connection between oligomerization and the final phase structure, we compare our findings to related studies reporting molecular dynamics (MD) simulations that illustrated the bridging process and the formation of rhombohedral crystal structural motifs. MD simulations showed that $[Bi_6O_4(OH)_4]^{6+}$ complexes in DMSO solution formed dimers *via* nitrite ion bridges and oligomerized further into $[Bi_6O_4(OH)_4](NO_3)_6$ clusters.[22,42,45,46] During the bridging process, two complexes were linked with rapidly formed temporary Bi–nitrite–Bi bonds with 1–3 nitrite bridges. Then these bonds quickly rearranged into Bi–O–Bi rhombohedral motifs with fourfold coordinated oxygen ions by Bi, characteristic to Bi_2O_3

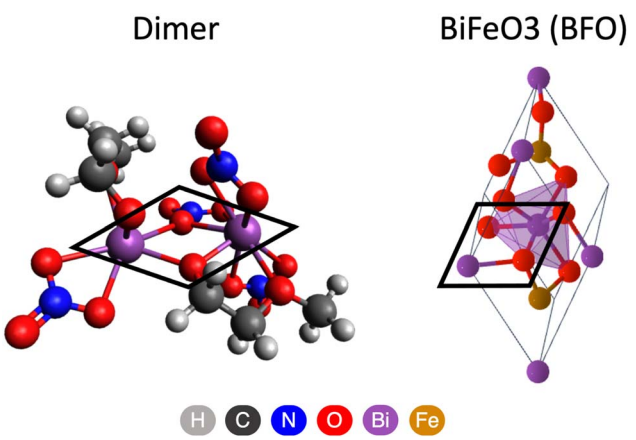

Fig. 5 Comparing rhombohedral motifs forming in the dimer structure during bridging and persisting in the BFO crystal.

 © 2025 The Author(s). Published by the Royal Society of Chemistry

Open Access Article. Published on 27 May 2025. Downloaded on 1/29/2026 3:29:41 AM.
This article is licensed under a Creative Commons Attribution 3.0 Unported Licence.

crystals.[42] These observations align with our findings and support our assertion that dimerization is the reaction pathway.

Next, we speculate on the potential implications of oligomerization being the favored pathway for the pure phase BiFeO3 formation, and particularly the effect of specific additive types in this process. We highlight that the following discussion is speculative and represents our attempt to connect all evidence reported in the literature, emphasizing that further research is needed. Our text-mining analysis reveals that only 2ME, ethylene glycol, and citric acid consistently lead to a pure phase (90 to 94% pure phase formation) while the addition of acetic acid derivatives, nitric acid, and surfactants, on average, decreasing the frequency of pure phase formation (66 to 68%). Previous studies suggest that impurity or amorphous phase formation may occur when competing chemical interactions are present within the precursor system.[1] Building on this, we hypothesize that the mentioned additives may initiate side processes, diverting from oligomerization — a preferential reaction pathway within the precursor solution, as shown in our CRN analysis.

Our results suggest that an increase in nitrite ions would favor oligomerization, as the driving force behind this process has been attributed to the presence of free nitrite ions in solution.[42] Surprisingly, our text-mining analysis showed that, in contrast to using pure nitrate salt, the addition of nitric acid decreases the formation of a pure phase. The reasons for this are unclear but may be related to excess nitrite competing with the solvent's ability to stabilize de-nitrated complexes. Previous MD simulations have shown that the ability of solvents to interact with under-coordinated Bi ions after nitrite ions depart is important for oligomerization.[42,45] See more discussion in ESI.†

The approach used in this work has several limitations. Extracting synthesis recipes from natural texts is a challenging task. A synthesis process is typically described in a concise manner, frequently containing missing steps and experimental parameters.[11,15] Also, the protocol complexity is not always explicitly described. To obtain a high-quality dataset, we extracted the synthesis recipes manually, which limited its size and influenced the range of conclusions we could derive. Advancements in automated text processing methods, such as large language models (LLMs), have effectively increased the volume of retrieved synthesis recipes; however, challenges remain in handling the versatility of features.[47]

The CRN method used in this work has several limitations, including: a minor trade-off in accuracy due to semi-empirical methods to manage the computational demand of data preparation with advanced structures like metal complexes; the use of the PCM solvation model; an inability to consider trimers due to the exponential increase in configurational conformers; and the inability to capture the complete chemical reaction pathway from individual molecules to final crystal formation. The primary limitation for this particular work is that we did not model Fe, due to its complex d-shell structure, which is not accurately accounted for by the semi-empirical methods used. We hypothesize that the Fe mechanism is similar to that of Bi based on experimental evidence. In the future, we hope these limitations will be overcome as methods progress.

5 Conclusions

This study presents a text-mining analysis of 340 sol–gel synthesis recipes for BFO precursor solution and crystallinity outcomes. Our analysis identified nitrates as the predominant metal salts and 2ME as the dominant solvent, with citric acid frequently leading to phase-pure BFO. The use of acetic acid and nitric acid as chelators resulted in variable phase purity, highlighting the complexity introduced by additional precursor materials.

The CRN analysis uncovered the initial parts of the pathway involved in the formation of BFO. The study found that the commonly proposed full solvation route, involving the complete replacement of nitrite ligands with 2ME ligands, is energetically unfavorable. Instead, a more plausible mechanism involves partial solvation followed by dimerization. Our findings explain existing studies, proposing that oligomerization is facilitated by nitrite ion bridging. This pathway aligns with experimental observations and suggests that oligomerization plays an important role in BFO phase seeding.

This work demonstrates the power of combining text-mining with CRN analysis to uncover the underlying mechanisms of complex synthesis processes.

This study has several future implications. Subsequent studies should investigate the role of different solvents and chelating agents in the synthesis of BFO, focusing on their impact on the reaction pathways and final crystal structures. The method described in this work can be applied to study synthesis of other complex oxides, enhancing their crystallinity and phase purity. Implementation of advanced text processing methods and CRN expansion would help to scale up to larger datasets and investigate more complex systems.

Data availability

The code for dataset generation and data analysis described in the article is publicly available and can be found at Zenodo at **https://doi.org/10.5281/zenodo.15389508**. The code for building a chemical reaction network *via* HiPRGen and the dataset used in the paper are publicly available and can be found at Zenodo at **https://doi.org/10.5281/zenodo.15389626**.

Author contributions

V. B.: conceptualization, methodology, software, investigation, data curation, writing – original draft, visualization. K. C.: data curation, formal analysis, writing – review and editing. M. T.: conceptualization, writing – review and editing C. S.-F.: conceptualization, supervision, writing – review and editing. G. C.: supervision, funding acquisition, writing – review and editing. A. J.: conceptualization, supervision, funding acquisition, project administration, writing – review and editing. S. B.: conceptualization, methodology, supervision, funding acquisition, project administration, writing – review and editing.

Open Access Article. Published on 27 May 2025. Downloaded on 1/29/2026 3:29:41 AM.
This article is licensed under a Creative Commons Attribution 3.0 Unported Licence.

Conflicts of interest

There are no conflicts to declare.

Acknowledgements

This work was partially funded and intellectually led by the U.S. Department of Energy, Office of Science, Office of Basic Energy Sciences, Materials Sciences and Engineering Division under Contract No. DE-AC02-05-CH11231 (D2S2 program KCD2S2). We acknowledge support by the Center for High Precision Patterning Science (CHiPPS), an Energy Frontier Research Center funded by the U.S. Department of Energy, Office of Science, Basic Energy Sciences at Lawrence Berkeley National Laboratory under contract DE-AC02-05CH11231. Computational resources were provided by the National Energy Research Scientific Computing Center (NERSC) and by the Lawrencium computational cluster resource provided by the IT Division at the Lawrence Berkeley National Laboratory. The Molecular Foundry supported by the Office of Science, Office of Basic Energy Sciences, of the U.S. Department of Energy under Contract No. DE-AC02-05CH11231 is acknowledged. We acknowledge U.S. Department of Energy (DOE), Office of Science, Office of Basic Energy Sciences, Heavy Element Chemistry Program (KC0302031) under contract number E3M2 and the LANL's Director's Postdoc Fellowship (LANL-LDRD, 20210966PRD4) (M.G.T.). We thank Andrew Rosen for support with QuAcc and for other valuable discussions.

Notes and references

1 Q. Zhang, D. Sando and V. Nagarajan, *J. Mater. Chem. C*, 2016, **4**, 4092–4124.
2 J. Wang, J. Neaton, H. Zheng, V. Nagarajan, S. Ogale, B. Liu, D. Viehland, V. Vaithyanathan, D. Schlom, U. Waghmare, *et al.*, *science*, 2003, **299**, 1719–1722.
3 P. Biswas, C. Thirmal, S. Pal and P. Murugavel, *J. Appl. Phys.*, 2018, **123**(2), 024101.
4 S. M. Selbach, M.-A. Einarsrud and T. Grande, *Chem. Mater.*, 2009, **21**, 169–173.
5 S. Pillai, D. Bhuwal, T. Shripathi and V. Shelke, *J. Mater. Sci.: Mater. Electron.*, 2013, **24**, 2950–2955.
6 F. Gheorghiu, M. Calugaru, A. Ianculescu, V. Musteata and L. Mitoseriu, *Solid State Sci.*, 2013, **23**, 79–87.
7 Y. Ma, W. Xing, J. Chen, Y. Bai, S. Zhao and H. Zhang, *Appl. Phys. A:Mater. Sci. Process.*, 2016, **122**, 1–9.
8 S. Gupta, M. Tomar and V. Gupta, *J. Mater. Sci.*, 2014, **49**, 5997–6006.
9 C. Anthony Raj, M. Muneeswaran, P. Jegatheesan, N. Giridharan, V. Sivakumar and G. Senguttuvan, *J. Mater. Sci.: Mater. Electron.*, 2013, **24**, 4148–4154.
10 M. Abdelsamie, K. Hong, K. Cruse, C. J. Bartel, V. Baibakova, A. Trewartha, A. Jain, G. Ceder and C. M. Sutter-Fella, *Matter*, 2023, **6**(12), 4291–4305.
11 K. Cruse, V. Baibakova, M. Abdelsamie, K. Hong, C. J. Bartel, A. Trewartha, A. Jain, C. M. Sutter-Fella and G. Ceder, *Chem. Mater.*, 2023, **36**, 772–785.
12 A. E. Danks, S. R. Hall and Z. Schnepp, *Mater. Horiz.*, 2016, **3**, 91–112.
13 D. Navas, S. Fuentes, A. Castro-Alvarez and E. Chavez-Angel, *Gels*, 2021, **7**, 275.
14 Q. Zhang, N. Valanoor and O. Standard, *J. Mater. Chem. C*, 2015, **3**, 582–595.
15 K. Cruse, A. Trewartha, S. Lee, Z. Wang, H. Huo, T. He, O. Kononova, A. Jain and G. Ceder, *Sci. Data*, 2022, **9**, 234.
16 O. Kononova, H. Huo, T. He, Z. Rong, T. Botari, W. Sun, V. Tshitoyan and G. Ceder, *Sci. Data*, 2019, **6**, 1–11.
17 M. J. McDermott, S. S. Dwaraknath and K. A. Persson, *Nat. Commun.*, 2021, **12**, 3097.
18 X. Xie, E. W. Clark Spotte-Smith, M. Wen, H. D. Patel, S. M. Blau and K. A. Persson, *J. Am. Chem. Soc.*, 2021, **143**, 13245–13258.
19 S. M. Blau, H. D. Patel, E. W. C. Spotte-Smith, X. Xie, S. Dwaraknath and K. A. Persson, *Chem. Sci.*, 2021, **12**, 4931–4939.
20 O. N. Temkin, A. V. Zeigarnik and D. Bonchev, *Chemical reaction networks: a graph-theoretical approach*, CRC Press, 2020.
21 A. Vaitkus, A. Merkys, T. Sander, M. Quirós, P. A. Thiessen, E. E. Bolton and S. Gražulis, *J. Cheminf.*, 2023, **15**, 123.
22 J. Näslund, I. Persson and M. Sandström, *Inorg. Chem.*, 2000, **39**, 4012–4021.
23 J.-T. Zhang, H.-Y. Wang, X. Zhang, F. Zhang and Y.-L. Guo, *Catal. Sci. Technol.*, 2016, **6**, 6637–6643.
24 M. Wen, E. W. C. Spotte-Smith, S. M. Blau, M. J. McDermott, A. S. Krishnapriyan and K. A. Persson, *Nat. Comput. Sci.*, 2023, **3**, 12–24.
25 M. Aykol, J. H. Montoya and J. Hummelshøj, *J. Am. Chem. Soc.*, 2021, **143**, 9244–9259.
26 J.-G. Sobez and M. Reiher, *J. Chem. Inf. Model.*, 2020, **60**, 3884–3900.
27 M. G. Taylor, D. J. Burrill, J. Janssen, E. R. Batista, D. Perez and P. Yang, *Nat. Commun.*, 2023, **14**, 2786.
28 Light-weight tight-binding framework, **https://www.github.com/tblite/tblite**.
29 E. Epifanovsky, A. T. Gilbert, X. Feng, J. Lee, Y. Mao, N. Mardirossian, P. Pokhilko, A. F. White, M. P. Coons, A. L. Dempwolff, *et al.*, *J. Chem. Phys.*, 2021, **155**(8), 084801.
30 A. S. Rosen, *QuAcc – The Quantum Accelerator*, Zenodo, 2023.
31 D. Barter, E. W. C. Spotte-Smith, N. S. Redkar, A. Khanwale, S. Dwaraknath, K. A. Persson and S. M. Blau, *Digital Discovery*, 2023, **2**, 123–137.
32 S. P. Ong, W. D. Richards, A. Jain, G. Hautier, M. Kocher, S. Cholia, D. Gunter, V. L. Chevrier, K. A. Persson and G. Ceder, *Comput. Mater. Sci.*, 2013, **68**, 314–319.
33 C. Zhu, R. H. Byrd, P. Lu and J. Nocedal, *ACM Trans. Math. Softw.*, 1997, **23**, 550–560.
34 C. Bannwarth, S. Ehlert and S. Grimme, *J. Chem. Theory Comput.*, 2019, **15**, 1652–1671.
35 Avogadro an open-source molecular builder and visualization tool. Version 1.2.0, **http://www.avogadro.cc/**.
36 N. Mardirossian and M. Head-Gordon, *J. Chem. Phys.*, 2016, **144**(21), 214110.

 © 2025 The Author(s). Published by the Royal Society of Chemistry

Open Access Article. Published on 27 May 2025. Downloaded on 1/29/2026 3:29:41 AM.
This article is licensed under a Creative Commons Attribution 3.0 Unported Licence.

37 A. Hellweg and D. Rappoport, *Phys. Chem. Chem. Phys.*, 2015, **17**, 1010–1017.
38 B. Mennucci, J. Tomasi, R. Cammi, J. Cheeseman, M. Frisch, F. Devlin, S. Gabriel and P. Stephens, *J. Phys. Chem. A*, 2002, **106**, 6102–6113.
39 P. A. Williams, A. C. Jones, M. J. Crosbie, P. J. Wright, J. F. Bickley, A. Steiner, H. O. Davies, T. J. Leedham and G. W. Critchlow, *Chem. Vap. Deposition*, 2001, **7**, 205–209.
40 D. T. Gillespie, *J. Comput. Phys.*, 1976, **22**, 403–434.
41 Z. Liu, H. Liu, G. Du, J. Zhang and K. Yao, *J. Appl. Phys.*, 2006, **100**(4), 044110.
42 M. Walther and D. Zahn, *Eur. J. Inorg. Chem.*, 2015, **2015**, 1178–1181.
43 M. Mehring, *Coord. Chem. Rev.*, 2007, **251**, 974–1006.
44 C. V. Thompson and R. Carel, *J. Mech. Phys. Solids*, 1996, **44**, 657–673.
45 M. Walther and D. Zahn, *Chem. Phys. Lett.*, 2018, **691**, 87–90.
46 M. Weber, M. Schlesinger, M. Walther, D. Zahn, C. A. Schalley and M. Mehring, *Z. Kristallogr. Cryst. Mater.*, 2017, **232**, 185–207.
47 A. M. Bran, S. Cox, O. Schilter, C. Baldassari, A. D. White and P. Schwaller, *Nat. Mach. Intell.*, 2024, 1–11.